Materials Research Bulletin 48 (2013) 1381–1387

Contents lists available at SciVerse ScienceDirect

Materials Research Bulletin

journal homepage: www.elsevier.com/locate/matresbu

Intermediate surface reactions to obtain nanocrystalline PbTe via high-energy milling

H. Rojas-Chávez [a,b,*], F. Reyes-Carmona [c], L. Huerta [d], D. Jaramillo-Vigueras [e]

[a] Instituto Tecnológico de Tláhuac–II, Camino Real 625, Col. Jardines del Llano, San Juan Ixtayopan, Del. Tláhuac México, D.F. 13508, México
[b] Centro de Investigación en Ciencia Aplicada y Tecnología Avanzada – IPN, Legaria 694, Col. Irrigación, Del. Miguel Hidalgo México, D.F. 11500, México
[c] Facultad de Química – UNAM, Circuito de la Investigación Científica s/n, C.U. Del. Coyoacan México, D.F. 04510, México
[d] Instituto de Investigación en Materiales – UNAM, C.U. Del. Coyoacan México, D.F. 04510, México
[e] Centro de Investigación e Innovación Tecnológica – IPN, Cerrada de CECATI s/n, Col. Santa Catarina, Del. Azcapotzalco. México, D.F. 02250, México

ARTICLE INFO

Article history:
Received 13 February 2012
Received in revised form 25 November 2012
Accepted 5 December 2012
Available online 31 December 2012

Keyword:
A. Nanostructures
A. Semiconductors
B. Chemical synthesis
C. Photoelectron spectroscopy

ABSTRACT

To elucidate how surface and gaseous phases interact each other to induce chemical reactions, X-ray photoelectron spectroscopy (XPS) analyses were carried out on powders as milling took place. An acute analysis of data acquired by the XPS-technique allowed us to find a series of well-defined chemical transitions from precursors to the stoichiometric PbTe phase. By coupling, theoretical and experimental data a self-consistent model was developed.

Initially, the process manifested itself as an oxidation stage and secondly as a reducing process. In agreement with a thermodynamic evaluation of free energy of phases traced during milling, chemical transitions were traced as Te^{2+} to Te^{6+} in oxidation reactions. If high oxygen potential prevails in the milling system subsequently Pb^{2+} evolves to Pb^{4+}. On the other way, high valence oxides like Pb^{4+} or Te^{4+} were reduced to Pb^{2+} and Te^{2-}. However, the last transition an asymmetric transformations was identified as non-stoichiometric phases.

1. Introduction

Previously, we have reported a chemical behavior of the Pb–O–Se ternary system. There, we pointed out that this ternary system presented three major reaction stages: (i) oxidation and reoxidation of precursors, (ii) chemical interaction between both Pb and Se suboxides in order to form a complex oxide and (iii) chemical reduction of that complex oxide to obtain PbSe nanocrystals [1]. However, on that work, it was not established why transformation kinetics from precursors to final products of PbTe and PbSe were quite different between them. Thus, while transformation in the Pb–O–Se system took about 10 h, milling time to processing PbTe was just about 4 h [1,2].

The high-energy milling (HEM) is a mean by which a series of reactions can be induced [1–4]. During particle size reduction bonds between atoms in a solid are: deformed, stressed and ultimately fractured; thus new surfaces are created. By fracture, atoms on the surface develop asymmetrical interactive forces which are characteristic of each substance. Since chemical bonds are out of balance on solid surfaces, reactiveness becomes quite high. Therefore, if two solid particles are in an intimate contact with each other or if a single surface particle is on contact with a gaseous phase, surface (chemically) reacts; these facts give way to a differential surface composition. Therefore, the HEM process promotes both solid–solid and gas–solid chemical reactions between precursors.

However, gas–solid reactions are the kinetic contributors that promote different rates of transformation [5]. It is worth to emphasize that just by solid–solid otherwise these reactions would not take place, or processing times would be much larger [1,3,5].

In order to understand why overall rate of transformation of PbTe is faster than PbSe, it is of prime importance to describe surface chemical reactions in the Pb–O–Te system. Thus, the purpose of present work is to elucidate how oxidation/reduction reactions in a mixture of PbO and Te micropowders as precursors evolve to form PbTe nanopowders. Nonetheless, processing by HEM involves both solid–solid and gas–solid surface chemical transformation, special attention is paid in this work to the latter chemical effects. Therefore, XPS studies were carried out on micro and on nanoparticles as well. Hence, a comprehensive model will be proposed. This model is based on dynamical equilibria where almost three chemical species are present to define the rates of transformations.

2. Experimental procedure

2.1. Sample preparation and ball milling treatment

A binary mixture of high purity micropowders of PbO (5 μm) and Te (50 μm) from Aldrich were used as precursors. The

* Corresponding author.
E-mail address: rojas_hugo@ittlahuac2.edu.mx (H. Rojas-Chávez).

0025-5408/$ – see front matter © 2012 Elsevier Ltd. All rights reserved.
http://dx.doi.org/10.1016/j.materresbull.2012.12.060

compound with nominal composition of Pb:Te was prepared by HEM. The PbO–Te powder mixtures were introduced in a vial under atmosphere conditions jointly with several ZrO_2-spheres. The HEM was carried out by using a SPEX mixer/mill model 8000. The ball-to-powder weight ratio was fixed at 10:1. The powder mixtures were introduced in a nylamid container under atmospheric conditions. The HEM was carried out for up to 4 h. Small amounts of the reaction mixtures were extracted at various times for further analysis.

Details about structural characterization of PbO–Te mixtures powders by XRD were reported elsewhere [3].

2.2. Scanning electron microscopy

At earlier stages of milling because of particle agglomeration, morphology changes were traced on these clusters by scanning electron microscopy. Microstructure evolution was conducted in a Hitachi S-570 scanning electron microscope with a Noran detector.

2.3. High-resolution transmission electron microscopy

Morphology and particle size were analyzed by high-resolution transmission electron microscopy in a FEI TECNAI G^2-F30 microscope. The as-milled powder was dispersed in ethanol before being placed in a copper grid covered with Formvar.

2.4. X-ray photoelectron spectroscopy

Stoichiometric and bonding changes in micro and nanocrystalline powders were monitored by core-level XPS studies.

XPS measurements were carried out using a VG Microtech ESCA2000 Multilab UHV system, with an Mg K_α x-ray source ($h\nu$ = 1253.6 eV), operated at 15 kV and 20 mA beam, and a CLAM4 MCD analyzer. In all cases, powder surface was etched during 5 minutes with 3.0 kV Ar^+ at 0.06 μA mm^{-2} to eliminate carbon debris. XPS spectrum was obtained at 55° to the normal surface in the constant pass energy mode (CAE), E_0 = 50 and 20 eV for survey and high resolution narrow scan, respectively. Peak positions were referenced to the background silver $3d_{5/2}$ photopeak at 368.20 eV, having a FWHM of 1.10 eV, Au $4f_{7/2}$ in 84.00 eV and C 1s hydrocarbon groups in 285.00 eV central peak position. The XPS spectra were fitted with the program SDP v 4.1 [6]. XPS error was based on a detection limit estimated to be 0.1% and uncertain propagation. For the deconvolution analysis the uncertainty degree estimated was 5%.

3. Results and discussion

3.1. Mechano-thermal effects traced by microscopy

XRD patterns of nanocrystalline PbTe powders contained all reflections planes characteristic of lead telluride [3]. In the PbO–Te system, powder mixtures were subjected to both solid-state and gas–solid reactions during HEM, as reported previously [1–3].

Fig. 1 shows SEM measurements. Fig. 1a indicates that there is not a visible structural refinement in the early milling times, it can be seen that there are larger particles. As milling time increases, agglomerates are clearly visible; see Fig. 1b. If the physical nature of precursors is taken into account, the broadest classification of the as-milling powders can be considered as ductile (PbO) and fragile (Te) phases, see Fig. 1c. Thus, PbO as the former and Te as the latter will behave as a structure capable to store a part of mechanical energy while the latter will consume another part of energy to generate, by fracture, a new surface area. Finally, as expected, since joining forces can be induced by different electrostatic charges induced by friction among powders or

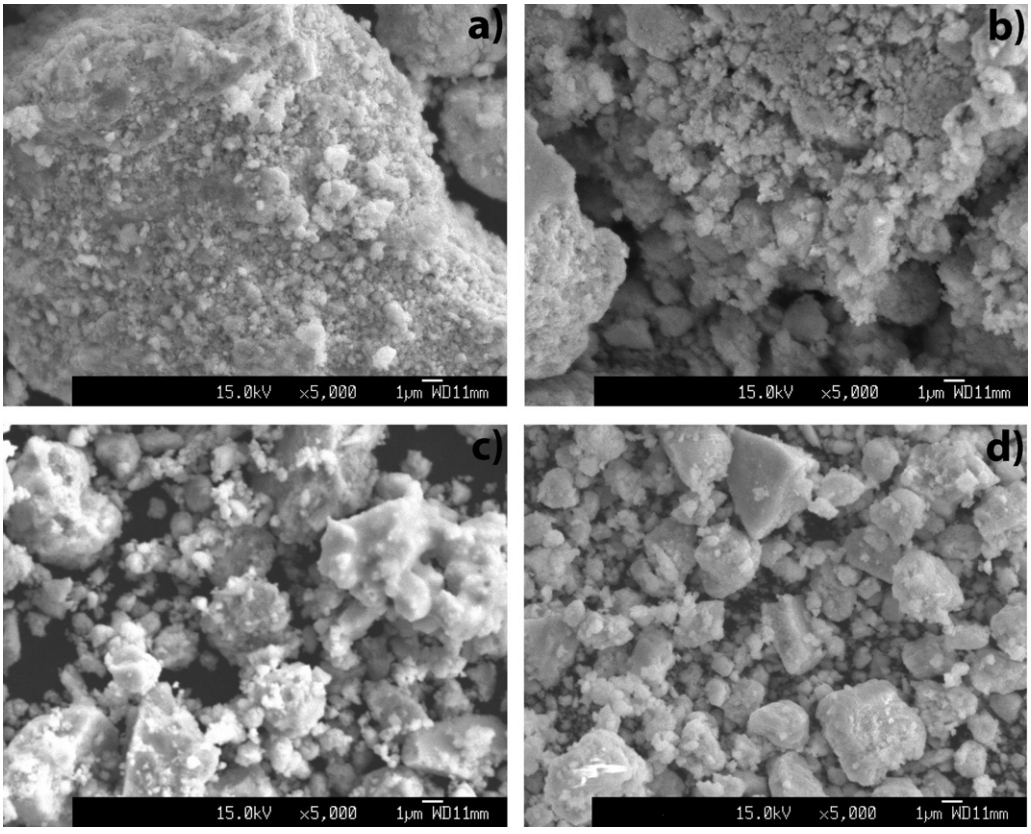

Fig. 1. SEM micrographs of the powders after: (a) 1, (b) 2, (c) 3 and (d) 4 h of milling.

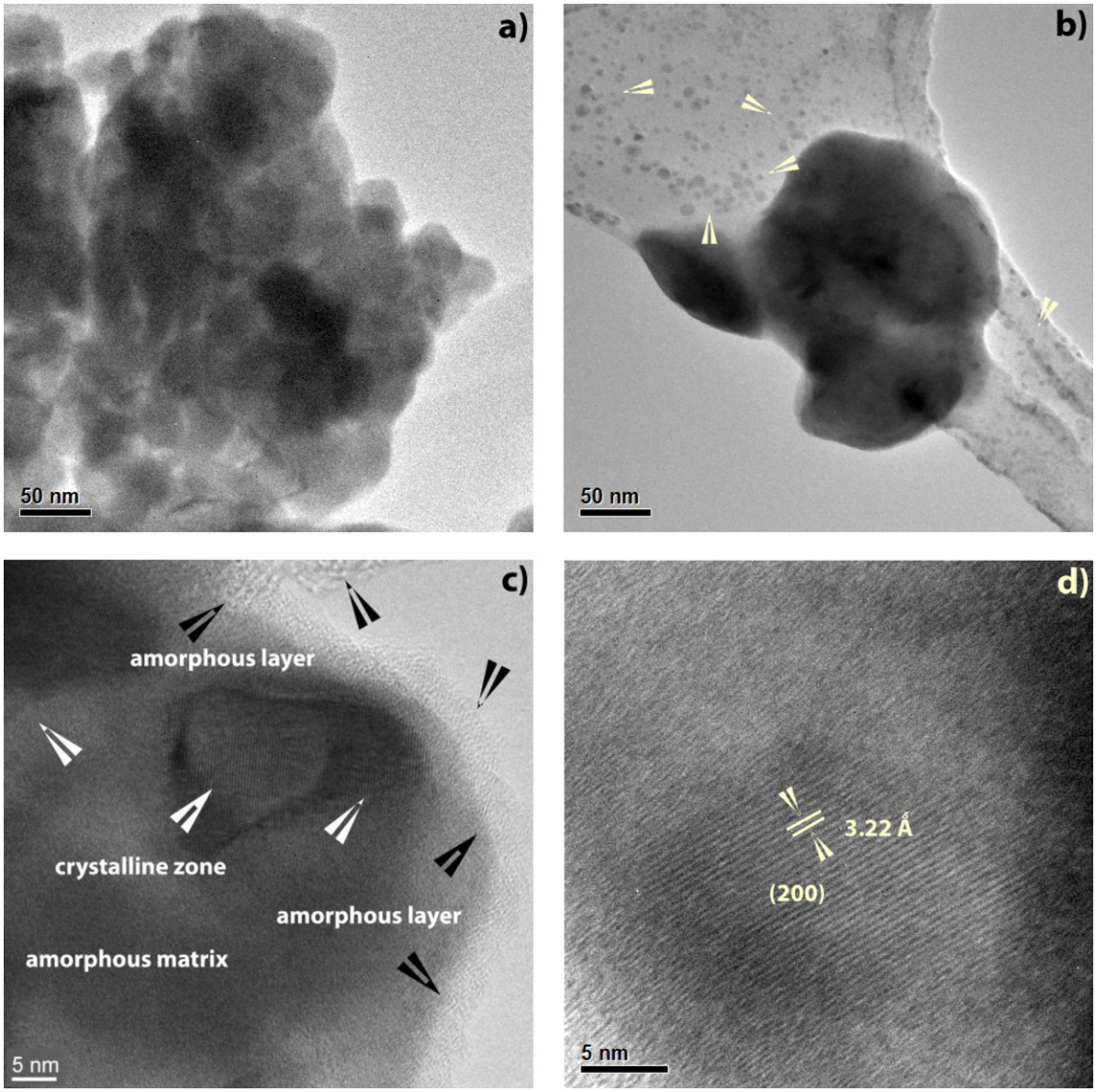

Fig. 2. HRTEM micrographs of PbTe powder after: (a) 1, (b) 2, (c) 3 and (d) 4 h of milling.

friction among powders and vial surfaces or even by low energy impact between ZrO_2-spheres and powders, the agglomerates will prevail; see Fig. 1d.

Fig. 2a shows a typical low resolution TEM micrograph of the powder milled for up to 1 h. As shown in this figure, large volumes of agglomerated nanoparticles do not exhibit well defined shape morphologies. However, as milling time increases up to 2 h, as shown in Fig. 2b, it becomes clearer that such agglomerates are integrated by several crystallites whose shape is hemispherical as pointed out by arrows in that Figure. Additionally, Fig. 2c shows a magnified image of a single particle when powders were processed for 3 h. It is covered by an amorphous layer as indicated out by black arrows. It is composed of an amorphous matrix in which nanosize crystalline particles are embedded as signaled by white arrows. Such arrangement of crystalline particles does not exhibit a well-defined morphology and their sizes range between 15 and 20 nm. TEM/EDS analyses performed on the PbTe particles, located within the amorphous matrix show that the Pb:Te atomic ratio of the PbTe is very close to 1:1. The Pb:Te ratio is close to 1:1 also in the amorphous matrix. However, occasionally the Pb:Te ratio was slightly greater than one.

Fig. 2d shows a HRTEM micrograph of powder milled after 4 h. As shown in this Figure, hemispherical crystalline particles have dimensions in the nanometric scale. Additionally, the lattice spacing traced by HRTEM shows that the *d*-spacing (3.22 Å) is consistent with that (3.2325 Å) expected for the (2 0 0) plane given by the 38-1435 JCPDS card.

To this point, it is necessary to remark the following facts: (*i*) particles are arranged as agglomerates, see Fig. 2a; (*ii*) crystallites are mainly hemispherical as indicated by arrows in Fig. 2b, (*iii*) there is a significant amount of amorphous phase as shown in Fig. 2c and (*iv*) hemispherical particles located on surface of agglomerates have already achieved the nanoscale size as shown in Fig. 2b and d.

3.2. X-ray photoelectron spectroscopy

In order to understand the bonding state of the as-milled products, XPS analyses of Te 3d, Pb 4f and O 1s spectra were performed. Surface composition of single: Te and PbO as-precursors, PbO–Te as a mixture and PbTe nanopowders were investigated by high resolution XPS. In every single case, the

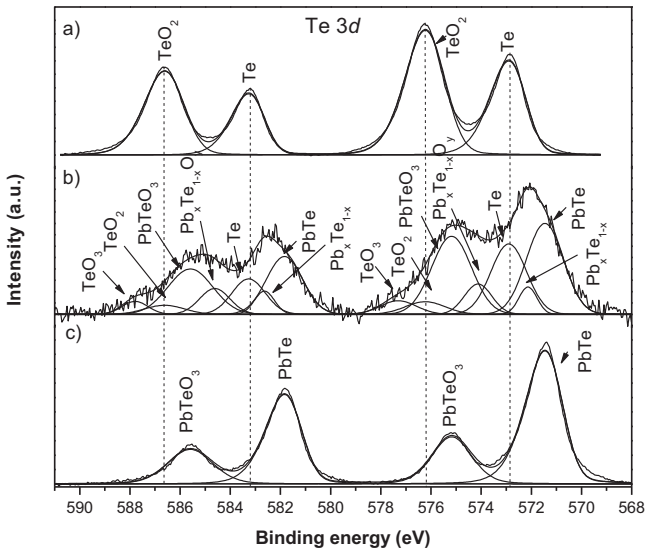

Fig. 3. XPS spectra of Te 3d core level: (a) Te as-precursor, (b) PbO–Te powder mixture, and (c) PbTe after 4 h of milling.

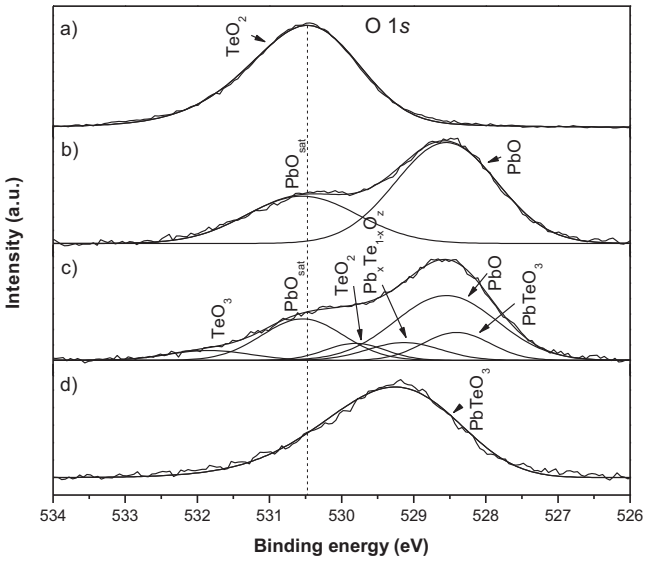

Fig. 5. XPS spectra of O 1s core level: (a) Te as-precursor, (b) PbO as-precursor, (c) PbO–Te powder mixture, and d) PbTe after 4 h of milling.

signals were fitted and deconvoluted to resolve these peaks. These results are shown in Figs. 3–5. The most probable bonding states of components are given in Table 1.

Fig. 3 depicts the fitted Te 3d core level spectra containing that observed with both PbO–Te mixture and PbTe. The difference between Te $3d_{5/2}$ and Te $3d_{3/2}$ is clearly resolved.

Fig. 3a displays the XPS spectrum of Te raw powders for Te 3d core level, the Te 3d spectrum consists of two peaks. These correspond to the 3d spin-orbit doublet. These findings confirm the presence of the tellurium alone and the tellurium as the oxide phase (Te–O) that corresponds to Te and TeO_2, respectively. Normally one would expect a core level shifted toward higher binding energies (BEs) by losing valence electrons. So, less electrons screen the coulomb potential and therefore, core electrons are bound on a stronger manner. Under an analogous argument, anions would have lower BEs as compared to normal atoms. Therefore, it is inferred that in the major peaks at higher energy Te is identified as (4+). A blue shift in the BE value of oxide related peaks suggests that Te has donated electrons to oxygen.

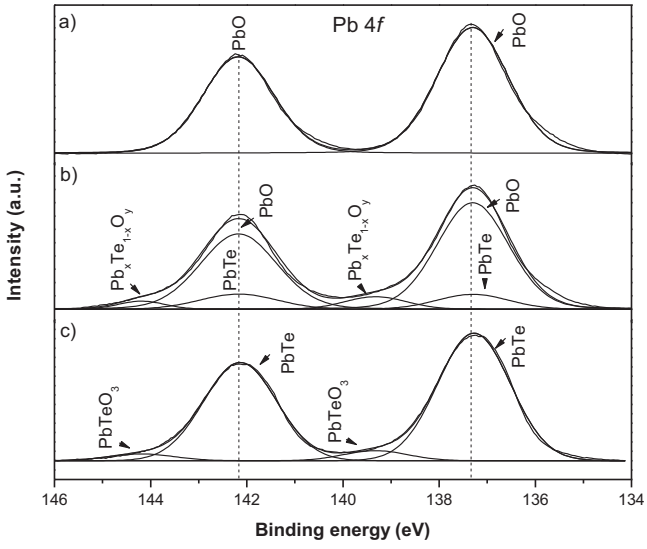

Fig. 4. XPS spectra of Pb 4f core level: (a) PbO as-precursor, (b) PbO–Te powder mixture, and (c) PbTe after 4 h of milling.

Therefore, the BE corresponding to Te 3d states has been increased as shown in Table 1.

By sputtering the Te as-precursor with Ar^+ ions, oxygen is not removed completely from Te surface due to its high oxidation susceptibility. However, oxide levels were not detectable by XRD [3]. The relative percentage of both element and compound as evaluated from the high resolution spectra using XPS peak fit software are 40% of Te and the TeO_2 oxide as a complement, i.e. 60%.

Fig. 3b displays the deconvoluted XPS spectrum of the PbO–Te powder mixture. It shows the characteristic Te and TeO_2 peaks at their corresponding BEs, see Table 1. However, a new set of components appear in the PbO–Te powder surfaces. In this case, powder sample undergoes three types of interactions, i.e. (i) Te–Pb, (ii) Te–O–Pb and (iii) Te–O. The first type represents phases with lower BEs as compared to elemental Te. In such case, there appear two peaks due to PbTe. In addition, closer to these two peaks there appear another couple of peaks that correspond to the Te 3d states. However, these do not strictly satisfy the one to one PbTe stoichiometric ratio instead this compound is represented by Pb_xTe_{1-x}. Thus, one can infer that in the major peak at lower energy Te is as (2−) and in the minor peak at higher energy Te would be even higher than (2−). Nonetheless, in the literature there is not reported any oxidation state for Te between 2− and 2+ [7]. For that reason, in the minor peak at higher energy Te is as (2−) as well. It means that, Te has accepted from Pb at least 2 electrons in these compounds. Therefore, the BE corresponding to Te 3d states has been diminished. The second type represents phases with higher BEs as compared to elemental Te. In such case, there appear two peaks that represent a non-stoichiometric $Pb_xTe_{1-x}O_y$ compound (where $x = 0.5$ and $0 \leq y \leq 3$) which resemble the $PbTeO_3$ [8–10]. Additionally, in adjacent locations to these two peaks there appears another set of peaks that represent the stoichiometric phase identified as $PbTeO_3$. Following a similar argument, in those complex oxides Te is traced as 2+, 4+ and up to 6+. Finally, the third type represents oxides with the highest BEs where an incipient presence of TeO_3 was traced. Thus, one can expect that in minor intensity peaks at the highest energy, Te may act as (6+). As a consequence, a blue shift in the BE value of oxide related peaks suggest that Te may have donated up to six electrons to oxygen. Therefore, the BE corresponding to 3d

Table 1
Assignments to the core level spectra of the high resolution surface XPS scans of Te as-precursor, PbO as-precursor, PbO–Te powder mixture, and PbTe after 4 h of milling.

Sample	Core level					Bonding state
	$4f_{7/2}$	$4f_{5/2}$	$3d_{5/2}$	$3d_{3/2}$	1s	
Te as-precursor	–	–	572.90	583.27		Te–Te
			576.23	586.62	530.48	Te–O
PbO as-precursor	137.30	142.17	–	–	528.54	Pb–O
					530.54	
PbO–Te mixture	137.30	142.17	571.46	581.84	528.41	
	139.32	144.19	572.13	582.64	528.55	
			572.90	583.27	529.13	Te–Te
			574.12	584.62	529.81	Pb–Te
			575.18	585.59	530.54	Pb–O–Te
			576.23	586.62	531.84	Te–O
			577.30	587.80		
PbTe nanopowders	137.27	142.14	571.46	581.84	529.26	Pb–Te
	139.32	144.19	575.17	585.59		Pb–O–Te

is the highest state by the Te, see Table 1. The relative percentage of the minor peaks corresponding to an oxide, as evaluated from the high resolution spectra using XPS peak fit software, is 4.4% of TeO_3. However, it is important to point out that such oxide was not detected by conventional XRD [3].

Fig. 3c displays the XPS spectrum of PbTe nanopowders. In this case, there appear two peaks that correspond to the PbTe phase. Additionally, close to these couple of peaks appears another set that are identified as complex intermediate oxide phase constituted by Te (Pb–O–Te). This complex oxide phase clearly corresponds to $PbTeO_3$. Thus, one can infer that in the major peaks at lower energy Te acts as (2−) and in the minor peaks at higher energy Te is postulated to be as higher than (2−) i.e. 4+ or even up to 6+. The relative percentage of compounds as evaluated from the high resolution spectra using XPS peak fit software are 71% of PbTe and the balance is that which corresponds to the $PbTeO_3$ compound.

Fig. 4 depicts the fitted Pb 4f core level spectra containing the PbO as-precursor with both the PbO–Te mixture and the PbTe-phase alone. Their data was fitted and deconvoluted to resolve the whole spectra of peaks. The difference between Pb $4f_{7/2}$ and Pb $4f_{5/2}$ is quite well resolvable. Fig. 4a displays the XPS spectrum of PbO as-precursor. This figure shows two peaks. A closer examination of BE value (Table 1) reveals that such peaks may be attributed to either PbO or PbO_2. Here, it is difficult to observe O component in Pb (4f) core level XPS spectra, since the BE difference between PbO and PbO_2 is only 0.1 eV. This difference is not sufficiently high to discern without a doubt the XPS of these phases. Therefore, one can infer that in such peaks Pb would represent Pb with either (2+) or (4+).

Fig. 4b displays the deconvoluted XPS spectrum of PbO–Te powders mixture. It shows the characteristic PbO or PbO_2 peaks at their corresponding BEs. We are able to fit three distinct components in the case of PbO–Te powders mixture. The major peaks correspond to either PbO or PbO_2. Also, the presence of two small peaks at the same BE of 137.30 and 142.17 eV that, as described earlier corresponds to the Pb 4f states. However, those must be attributed to the PbTe phase. Additionally, there is a significant amount of the component corresponding to the higher BE of 139.32 and 144.19 eV; that, as indicated previously, corresponds to Pb 4f states. However, it should be pointed out that this compound do not show a well-defined stoichiometric ratio, instead it obeys to the following atom distribution, $Pb_xTe_{1-x}O_y$ [8,9]. Based on earlier statements one can infer that, peaks that represent the same BE for Pb acts as (2+) whereas in the peaks at higher BE Pb can change from 2+ up to 4+. A careful interpretation of these signals should be pertinent, since the PbO peak in these signals appears superposed on the PbTe peak as shown in Fig. 4b. The relative percentage of compounds (as valued from the high resolution spectra using XPS peak fit software) are: 80.8% of PbO (1:1 or 1:2 ratio), 12.8% of PbTe and the difference of the non-stoichiometric oxide designed as: $Pb_xTe_{1-x}O_y$.

Fig. 4c displays the XPS spectrum of PbTe nanopowders. This figure shows two peaks at 137.27 and 142.14 eV that correspond to $4f_{7/2}$ and Pb $4f_{5/2}$. This is attributed to the PbTe phase. Additionally, two peaks appear at higher BE of 139.32 and 144.19 eV. These peaks correspond to Pb in 4f states. However, through these states it can be identified the intermediate oxide, $PbTeO_3$. The peak at lower energy is the major one, this indicates that Pb acts as (2+) whereas in the small peak at higher energy Pb would be as either (2+) or (4+). The relative percentage of compounds as evaluated from the high resolution spectra using XPS peak fit software are: 94% of PbTe and the difference of $PbTeO_3$.

Fig. 5 depicts the fitted O 1s core level spectra containing: Te and PbO as-precursors, PbO–Te as a mixture and PbTe nanopowders; fitted and deconvoluted to resolve the peaks. These data are disclosed as follow:

Fig. 5a displays the XPS spectrum of Te as-precursor. It exhibits a single peak at 530.48 eV which corresponds to TeO_2. Meanwhile in Fig. 5b corresponding to PbO as the second precursor, there appeared two peaks at 528.54 and 530.54 eV where these peaks correspond to PbO and its satellite, PbO_{sat}.

Fig. 5c displays the deconvoluted XPS spectrum of PbO–Te powders mixture. It shows the characteristic PbO and TeO_2 peaks at their corresponding BEs and a set of new peaks appeared. We are able to fit three distinct O 1s peaks i.e. 528.41, 529.13 and 531.84 eV. Thus, one can postulate that the peak with the highest BE to the oxygen associated with the Te–O bond is that which corresponds to TeO_3; the BE of 529.13 eV resulted from the oxygen, that is associated to Pb–O–Te and it corresponds to non-stoichiometric compound represented by $Pb_xTe_{1-x}O_z$ (where $x = 0.5$ and $3 \leq y \leq 4$), and an O 1s peak at 528.41 eV was due to the $PbTeO_3$, respectively. However, it is important to point out that $Pb_xTe_{1-x}O_z$ was incipiently traced by the XPS technique. Finally, in Fig. 5d it may be observed that the PbTe sample surface composition is only due to $PbTeO_3$ and it appears at BE of 528.41 eV.

Compared with other lead chalcogenides, such as PbS and PbSe, the PbTe surface is more susceptible to form a surface layer of either Pb or even Te suboxides. This phenomenon can be attributed to tellurium having a more metallic character than sulfur or selenium [8]. On the other hand, it is interesting to note that with either Pb:O or Pb:Te ratio 1:1, the full width at half maximum (FWHM) remains the same, indicating similar chemical

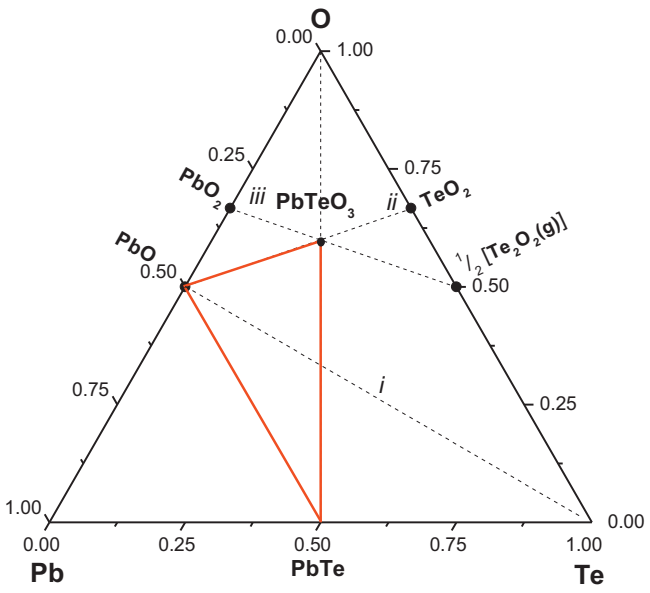

Fig. 6. Ternary representation of the: (i) initial stage during milling, (ii) simultaneous oxidation/reduction process during early stages of milling where the initial transformation generate the PbTe phase, and (iii) The gaseous specie, ½ [Te_2O_2], undergoes a reoxidation to form the TeO_2 as the milling time increases.

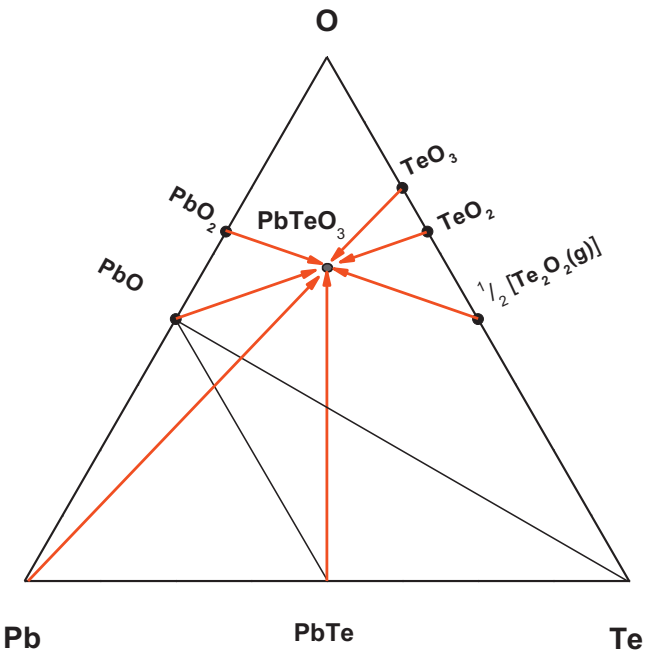

Fig. 7. Contributions of phases to the formation of the pivot point, dynamic equilibrium, represented by $PbTeO_3$. This point represents the average maximum oxygen potential developed during milling.

environment for either Pb in PbO microparticles or Pb in PbTe nanoparticles.

Thus, we found that both PbTe and Te surface powders are easily oxidized either Te^{2-} or Te° are partially oxidized to the Te^{4+} or even Te^{6+} state. This finding is quite interesting, since the percentage Te^{4+} on both PbTe and Te powder surfaces significantly depends on the oxygen atmosphere exposure. It is worth mentioning that present XPS experimental results suggest that the %Te^{4+} on Te surface powders is high. However, its level is not detectable by XRD [3]. Therefore, a similar statement can be applied to the PbTe nanopowders.

3.3. Chemical interpretation of local surface analysis

In order to show graphically how powders transform chemically from precursors as micropowders to nanoparticles of high crystalline purity, a couple of ternary diagrams are disclosed. These changes are shown as transformations comprised within at least two constituents as shown in Figs. 6–7. The initial stage is that which represents the chemical potential of micropowders as precursors, in respect to PbTe, in the vial. Those contributing phases that rule the oxygen potential are shown in Fig. 6 (line *i*). A very decisive fact to be mentioned is that precursors were charged under atmosphere conditions and either physisorbed or chemisorbed oxygen containing phases in the whole milling system were not attempted to be removed by any means.

Based on previous statements, the first stage as indicated by the XPS-analysis as well as by conventional XRD [3], represents surface simultaneous oxidation/reduction process is where the most stable gaseous phase manifest itself as Te_2O_2 (g) [11]. And, as shown in Fig. 6 (line *ii*), this gaseous phase is plotted as ½ [Te_2O_2]. The transformation, even at the most incipient milling conditions, starts to generate the intermetallic phase, PbTe. The following part of the transformation induced by milling is that also represented in Fig. 6 (line *iii*). There, we note that as processing time increases the reoxidation process tends to reach that stage given by the TeO_2. However, the oxygen potential solely manifests itself as an intermediate stage that lies between PbO and TeO_2.

Fig. 7 shows both the most stable phase found during the whole milling process, $PbTeO_3$; and the threefold condition where all PbO, $PbTeO_3$, and PbTe may coexist during the most important and the longest transformation time. Those contributing phases that rule the oxygen potential are shown in Fig. 7. To this point, it is worth emphasizing that $PbTeO_3$ can be a consequence of multiple contributions, PbO–TeO_2 subsystem, like PbTe + $^3/_2$ O_2, PbO_2 + ½ Te_2O_2 and including TeO_3 + Pb. However, although PbO_2 and TeO_3 might be traced to a minimum extent by XPS technique, it must be important to stipulate that the most stable tellurium oxide phase is that where tellurium acts mainly as a tetravalent species [3].

The final transient of the transformation involves the following phases [9,12]:

$PbTeO_3$, PbTe, Te_2O_2 (g), 'Pb_2O'
'$PbTeO_2$', Te, Te_2O_2 (g), Pb and ½ O_2 (g)

Notice that '$PbTeO_2$' is not a stable phase reported. However, it is important to point out that just before the nanocrystalline PbTe phase was detected; in the last transient stage the characteristic chemical transitions was represented by both amorphous and non-stoichiometric phases. These findings indicate us that unsteady state conditions are chemically unstable transitions as well, where Te changes its oxidation state. Therefore, the non-stoichiometric phases have to be expected to see as amorphous reaction products, namely $Pb_xTe_{1-x}O_y$ or even $Pb_xTe_{1-x}O_z$.

4. Conclusions

HRTEM analysis revealed that samples were affected by physical parameters such as: (i) friction, (ii) Van der Waals' forces and (iii) cold welding. The effects were macroscopically traced as agglomerated nanoparticles, as shown via SEM.

The XPS analyses show that significant amounts of stoichiometric and non-stoichiometric phases are always present on powder surfaces. Surface oxidation in PbTe powders only give way to $PbTeO_3$ whereas in PbO–Te powder mixture both

$Pb_xTe_{x-1}O_y$ and $Pb_xTe_{x-1}O_z$ were traced. The charge state of Te appears to be: less than 4+ in the non-stoichiometric $PbTe_xO_{1-x}$; 4+ in the stoichiometric $PbTeO_3$ and higher than 4+ in the non-stoichiometric $Pb_xTe_{x-1}O_z$ (less than 6+). These results indicate themselves that strong chemical interactions between oxygen and surface powders can take place. These set of reactions are comprehensively represented either as twofold or threefold interaction of phases located within a major Pb–O–Te ternary diagram. However, the most meaningful binary subsystem where the chemical transitions occur and are those framed in the PbO–TeO_2 oxide subsystem. Hence, the specific phase that hinge redox reactions is that stoichiometric phase given by $PbTeO_3$ ($PbO{\cdot}TeO_2$).

Acknowledgements

This study was partially supported by the Consejo Nacional de Ciencia y Tecnología de México (CONACyT). One of the authors (H. Rojas-Chávez) would like to thank CONACyT for the *financial support extension*. The authors are grateful to Dr. F.J. Rodríguez-Gómez (IQ-UNAM) and Dr. V. Garibay-Flebes (IMP) for their technical support.

References

[1] H. Rojas-Chávez, F. Reyes-Carmona, et al. Mater. Res. Bull. 46 (2011) 1560–1565.
[2] H. Rojas-Chávez, S. Díaz-de la Torre, et al. J. Alloys Compd. 483 (2009) 275–278.
[3] H. Rojas-Chávez, F. Reyes-Carmona, D. Jaramillo-Vigueras, Rev. Metal. Madrid 46 (6) (2010) 548–554.
[4] M. Saleemi, M.S. Tropak, et al. J. Mater. Chem. 22 (2012) 725–730.
[5] J.J. Moore, Chemical Metallurgy, Butterworths, London, 1990.
[6] SDP v4.1 (32 bit) Copyright© 2004, XPS International, LLC, Compiled in January 2004.
[7] B. Murphy, C. Murphy, B.J. Hathaway, Basic Principles of Inorganic Chemistry, The Royal Society of Chemistry, UK, 1998.
[8] J. He, S. Mao, S. Zhang, et al. Mater. Sci. Semicond. Process. 12 (6) (2009) 217–223.
[9] J. Galat, J. Haber, J. Nowotny, et al. Oxid. Met. 9 (6) (1975) 497–506.
[10] Z. Dashevsky, E. Shufer, V. Kasiyan, et al. Physica B 405 (2010) 2380–2384.
[11] I. Barin, Thermochemical Data of Pure Substances, 3rd ed., Weinheim, VCH, New York, 1995.
[12] L. Chen, T. Goto, et al. 16th International Conference on Thermoelectrics, IEEE, 1997.